From a localized H_3O radical to a delocalized $H_3O^+ \cdots e^-$ solvent-separated pair by sequential hydration†

Frank Uhlig, Ondrej Marsalek, and Pavel Jungwirth*

Abstract

The impact of microhydration on the electronic structure and reactivity of the H_3O moiety is investigated by ab initio calculations. In the gas phase, H_3O is a radical with spin density localized on its hydrogen end, which is only kinetically stable and readily decomposes into a water molecule and a hydrogen atom. When solvated by a single water molecule, H_3O preserves to a large extent its radical character, however, two water molecules are already capable to shift most of the spin density to the solvent. With three solvating water molecules this shift is practically completed and the system is best described as a solvent-separated pair of a hydronium cation and a hydrated electron. The electronic structure of this system and its proton transfer reactivity leading to formation of a hydrogen atom already resemble those of a proton-electron pair in bulk water.

Institute of Organic Chemistry and Biochemistry, Academy of Sciences of the Czech Republic and Center for Biomolecules and Complex Molecular Systems, Flemingovo nám. 2, 16610 Prague 6, Czech Republic; Tel: +420 220 410 314; E-mail: pavel.jungwirth@uochb.cas.cz

† Electronic Supplementary Information (ESI) available: Animation of reaction presented in Fig. 7. See DOI: 10.1039/b000000x/

1 Introduction

The strength of hydrogen bonding interactions between polar or ionic solutes and the solvating water molecules depends on the polarity and/or charge density of the dissolved species. From this perspective, a rather complex situation can occur when the electronic structure of the solute changes significantly upon hydration. In general, the highly polar water molecules tend to induce an increase in the polarity of the solute whenever its structure is sufficiently flexible to allow for such a change. An interesting example of such a shift in electronic structure upon hydration is the H_3O radical, which has been suggested to be one of the key species involved in radiation chemistry processes in water.[1–6] This is a well-justified suggestion, but needs some clarification concerning the exact nature of this radical when interacting with water molecules. It was shown that in water a ground state radical with spin density localized at the H_3O moiety does not exist.[3,6,7] Instead, this species acquires the form of a solvent-separated $H_3O^+ \cdots e^-$ pair, which raises the question whether it is actually adequate to call it an H_3O radical when dissolved in water. A solvent-separated $H_3O^+ \cdots e^-$ pair is only kinetically stable, rapidly forming a hydrogen atom.[3,7] The proton-electron reaction is one of the fundamental processes in radiation chemistry of water.[8] It was shown both experimentally[9,10] and computationally[7] that this reaction is not diffusion limited, exactly because of the formation of the solvent-separated $H_3O^+ \cdots e^-$ pair, and that it proceeds as proton transfer rather than electron transfer. Moreover, calculations did not point to a localized H_3O radical as a reactive intermediate during this process.[7] In other words, the rate-limiting process of the reaction is not the proton-electron recombination step but rather the deformation of the immediate solvent shell of the hydrated electron induced by the presence of the excess proton.[7]

For the gas phase radical the spin density must be localized on the H_3O moiety simply because there is no solvent to pass it to. Additionally, previous calculations showed that already 3 water molecules are sufficient to completely transfer the spin density from the H_3O to the solvent.[3,6,11] From this perspective it is of interest to explore the process of microhydration of H_3O. In the present study we investigate using ab initio quantum chemical methods clusters containing H_3O with up to 3 water molecules focusing on two mutually interconnected issues. The first one involves the gradual loss of the localized radical character of H_3O upon adding the first, second, and third water molecule. The second one concerns the reactivity leading to the loss of a hydrogen atom, either directly from the original H_3O moiety or indirectly via proton transfer to a water molecule involved in solvating the highly mobile excess electron.

2 Methods

We performed geometry optimizations and minimum energy path (MEP) calculations for differently sized $H_3O(H_2O)_n$ clusters, with n = 0–3. For the main part of the results, the electronic structure was calculated using the Møller-Plesset perturbation theory in the resolution of identity approximation (RI-MP2) in its spin-unrestricted formulation using Dunning's correlation-consistent triple-ζ split valence basis set augmented with diffuse functions (aug-cc-pVTZ)[12]. The TURBOMOLE[13] program package was used for all RI-MP2 calculations.

Geometry optimizations, relaxed scans of the potential energy surface (PES), and nudged elastic band (NEB)[14] calculations were performed using the above electronic structure method. Geometries of the local minima of the clusters were optimized with the Broyden-Fletcher-Goldfarb-Shanno (BFGS) algorithm.[15–18] MEPs for hydrogen abstraction from the clusters with n=0, 1, 2 were obtained as relaxed PES scans, where the individual structures were optimized using the FIRE algorithm[19]. NEB calculations calculations were performed for the clusters with two (16 images) and three (32 images) water molecules. A climbing image was used to ensure that one of the images is the transition state.[20] The FIRE algorithm was used for the optimization of the band. In the NEB method, a series of replicas of the system lying between the reactant and product states is connected atom-by-atom using harmonic bonds. Further, forces from the additional harmonic bonds perpendicular to the direction of the band are removed, preventing the band from "cutting corners". All the replicas are optimized simultaneously under the influence of both normal forces and forces from the harmonic bonds. The endpoints of the NEB were two local minima — one structure with the hydronium cation and the hydrated electron separated by solvent molecules and another with a hydrogen atom bound non-covalently to a relaxed cluster of two or three water molecules. Initial positions of the intermediate images were taken from the converged DFT calculations (see below). All these optimizations were performed using the Atomic Simulation Environment (ASE)[21]. Its interface to TURBOMOLE was modified to enable RI-MP2 calculations.

To check the effect of additional dynamic correlation we also performed CCSD(T) calculations employing the same aug-cc-pVTZ basis set on top of the RI-MP2 geometries of the hydrogen abstraction path in H_3O. The CCSD(T) calculations were carried out using the NWCHEM program package.[22]

In addition, benchmark calculations were performed using energies and forces obtained with density functional theory (DFT). We used the Becke, Lee, Yang and Parr (BLYP) exchange-correlation functional[23,24] with additional, pairwise additive London terms effectively accounting for dispersion effects.[25] We employed the scaled self-interaction correction (SIC) applied only to the singly-occupied orbital in a restricted open-shell calculation.[26] The scaling parameters

used were a=0.3 and b=0.2, as previously parametrized for the proton-electron reaction in a cluster of 32 water molecules[7]. Other values were used as well for comparison purposes. A hybrid Gaussians and plane waves (GPW) scheme was used, where the Kohn-Sham orbitals are represented as a linear combination of Gaussian basis functions, while the electronic density is represented in a plane-wave basis. In this work, a molecularly optimized generally contracted triple-ζ basis set with two additional polarization functions (molopt-TZV2P) was used as the atom-centered Gaussian basis set[27], possibly extended by a grid of Gaussian functions denoted as ggg.[7,28] The plane-wave cutoff for the density was set to 280 Ry and the Goedecker-Teter-Hutter norm-conserving pseudopotentials were employed.[29] A wavelet-based Poisson solver was used for correct treatment of electrostatics in open boundary conditions.[30] Although BLYP is generally not as accurate as MP2, this setup, once benchmarked properly, can be applied to much larger cluster systems as well as condensed phase problems.[7]

This electronic structure setup was used for NEB calculations of hydrogen abstraction from clusters with two and three water molecules. Improved tangent estimates[31] were used for better stability and a climbing image[20] was used to obtain the transition state. The band was optimized using molecular dynamics with the projected velocity Verlet modification of the propagator.[32] This propagator works in the same way as the original one used for molecular dynamics, but in addition, the relative direction of velocities and forces is checked in each step using a dot product. If the direction is opposite, velocities are set to zero. The endpoints of the NEB were prepared the same way as in the RI-MP2 setup. Initial conditions for the intermediate images were created by linear interpolation between the endpoints and one configuration in the vicinity of the transition state taken from a relaxed PES scan. All DFT-based calculations were performed with the CP2K program suite and its Quickstep module.[33]

3 Results and Discussion

First, we focus on consequences of microhydration of the central H_3O moiety for its electronic strcuture. To this end we performed geometry optimizations of the $H_3O(H_2O)_n$ clusters with n = 0–3, leading to the structures shown in Fig. 1. Starting geometry of the largest $H_3O(H_2O)_3$ cluster was taken from ref. 2, while for $H_3O(H_2O)_n$ with n=0, 1, 2 they were obtained by sequentially removing water molecules from the $H_3O(H_2O)_3$ cluster. These optimization yielded structures (A), (C), (D), and (E). Except for structure (D), these were previously reported as the local minima lowest in energy with the constraint of preserving the hydronium species intact (i.e., non-dissociating).[11] Note that structure (D) is 0.19 eV higher than the lowest local minimum with a preserved hydronium geometry for that system (which has a central water

molecule with H_3O on one side and H_2O on the other)[11]. In addition, we separately constructed and optimized a previously unnoticed structure (B), which has a water molecule donating rather than accepting a hydrogen bond, and which is about 0.30 eV higher in energy than structure (C).

Fig. 1 provides also graphical information on the electronic structure in terms of the unpaired spin density for each system. In isolated H_3O, the spin density of the system is localized on the hydrogen atoms and, to a lesser extent, also on the oxygen of the H_3O radical. The vertical ionization potential (VIP) of the isolated H_3O radical amounts to 5.88 eV (Tab. 1). Comparing the two structures with a single solvating water molecule, one can clearly see the difference between hydronium accepting a hydrogen bond from a water molecule and that donating a hydrogen bond to a water molecule. In the former case, hydronium remains practically intact as a spin-localized H_3O radical with only a slightly reduced VIP of 5.65 eV (structure (B) in Fig. 1 and Tab. 1). In the latter case, however, the spin density distorts (structure (C) in Fig. 1), leading to a significant reduction of the VIP to 4.56 eV (Tab. 1). Just as the first water molecule, the second and the third one also prefer to attach to the hydrogen side of the H_3O species (Fig. 1). In the process of increasing the number of solvent molecules in the cluster, the spin density further leaks away from H_3O and localizes near the dangling hydrogens of the water molecules. Already for two added water molecules, there is very little spin density left on the original H_3O radical (structure (D) in Fig. 1) and, consequently, the VIP further drops to 4.11 eV (Tab. 1). For three water molecules hydrating H_3O, the spin transfer to the solvent is practically completed. Hence, the hydronium loses its radical character and becomes a cation, donating hydrogen bonds to the surrounding water molecules. The excess electron localizes on the opposite side of the cluster between the free OH bonds. Thanks to the stabilization by the dangling water hydrogens, as well as by the presence of the H_3O^+ cation, the excess electron in the cluster with three water molecules already qualitatively resembles in its size and binding energy (4.09 eV) a bulk hydrated electron.

The gradual shift from an H_3O radical toward a solvent-separated $H_3O^+ \cdots e^-$ pair affects also the reactivity of this species, as demonstrated on the minimum energy paths for the dissociation of $H_3O(H_2O)_n$ to $(H_2O)_{n+1} + H$. The isolated H_3O radical can only dissociate by breaking one of its OH bonds. The energy profile of this process, obtained from a relaxed PES scan, is depicted in Fig. 2. In order to validate the employed RI-MP2 method, we compare it to CASPT2 calculations with a comparable basis set, taken from ref. 2, and, for comparison, we also present UHF results. Note that the CASPT2 method accounts for both static and dynamic correlation, while RI-MP2 essentially only for the latter. The bond lengths reported at the minimum are 1.01 Å with RI-MP2 and 0.98 Å for CASPT2. At the transition state the OH bonds are 1.2

and 1.19 Å and the barrier heights 0.11 and 0.13 eV, respectively. Also shown in Fig. 2 are CCSD(T) energies (red) calculated for the geometries obtained from the RI-MP2 relaxed scan. The close match in geometries and relative energies between CASPT2 and RI-MP2, as well as the non-negligible mismatch with the UHF results illustrates that for the cleavage of an OH bond of the H_3O radical, it is dynamic correlation that primarily needs to be accounted for. On the basis of the very good match between CCSD(T) and RI-MP2, especially in the transition state region, we can conclude that RI-MP2 is fully sufficient in describing the correlation effects in our systems. This conclusion has also been verified in previous studies for isolated H_3O, as well for the $H_3O(H_2O)_3$ cluster[1,34] and is in agreement with the observation that "the ground state of the hydronium radical is dominated by a single reference".[1] SIC-DFT (a=0.3, b=0.2) with molop-TZV2P+ggg basis underestimates the barrier of the reaction (0.03 eV) in contrast to RI-MP2 or CCSD(T).

By adding one water molecule that donates a hydrogen bond to H_3O the formation of a hydrogen atom is only favourable via the dissociation of an OH bond of the H_3O radical (Fig. 3). The energetics of the dissociation are essentially the same as for the isolated H_3O radical. The minimum is located at OH bond length of 1.02 Å, the maximum at 1.18 Å and the barrier height is 0.08 eV. In contrast, dissociation of an OH bond of the water molecule donating a hydrogen bond to the H_3O radical proceeds only over a high barrier of 5.22 eV until the whole cluster undergoes rearrangements to form an H_2O dimer and a hydrogen atom. In the cluster with the H_3O radical donating a hydrogen bond to a water molecule, there are two practically identical low-barrier ($\sim$0.1 eV) pathways leading again to the formation of a hydrogen and a water dimer (Fig. 4). We can conclude that in both $H_3O(H_2O)$ clusters the lowest reaction paths are analogous to that in the H_3O radical.

For clusters containing more than one water molecule, the OH bond dissociation at the H_3O moiety is not favorable. In the $H_3O(H_2O)_2$ cluster, only one hydrogen of the H_3O does not form a hydrogen bond to a water molecule. For dissociation of the corresponding OH bond a barrier of about 0.22 eV has to be overcome, which is mainly due to necessary rearrangements of the cluster. The favorable process is, however, the dissociation of a water OH bond, which proceeds over a small ($<$0.1 eV) barrier connected with the proton transfer from H_3O to the water molecule. The almost simultaneous cleavage of the water OH bond which has the hydrogen atom penetrating into the excess electron density is practically barrierless. In contrast, the other water OH bond does not break so easily, since the cluster needs to rearrange first with respect to the excess electron. In these cases, the reaction proceeds via structures which have a highly distorted, but compact excess electron.

A simple bond distance is not the best choice of a reaction coordinate for hydrogen abstrac-

tion reactions in clusters with more than one water molecule since it does not capture very well collective motion — relaxation of the whole cluster or coordinated transfer of two protons. One demonstration of this problem is the lack of smoothness in the reaction profiles presented in Fig. 5. In order to obtain the intrinsic reaction coordinate of these more difficult reactions, we performed calculations using the NEB method.[14]

For hydrogen abstraction from the $H_3O(H_2O)_2$ cluster, a total of 16 NEB images were used to obtain the MEP. Specifically, the OH bond to be dissociated corresponds to the green curve in Fig. 5. This choice corresponds to the OH bond that most significantly points into the electronic cloud of the excess electron. It was motivated by the fact that it shows the lowest barrier in the relaxed PES scans presented above and is, therefore, decisive for the stability of this cluster. RI-MP2 energies along the resulting MEP are shown in the top panel of Fig. 6 together with snapshots of selected configurations. In contrast with the case of the relaxed scan, the MEP obtained using NEB is smooth in energies and geometries. Moreover, as the climbing image extension of the NEB method was used, one of the replicas is in the transition state, which gives a good estimate of the barrier height. The barrier is negligible (5 meV) and would be practically non-existent if quantum nuclear effects were taken into account. The bottom panel of Fig. 6 shows relevant distances between atoms taking part in the reaction as a function of the reaction coordinate. The largest rate of change of all of these coordinates can be seen in the vicinity of the transition state.

The MEP for hydrogen abstraction from the $H_3O(H_2O)_3$ cluster was evaluated in two steps. First, a rough estimate of the reaction path was calculated using 8 images. These were then used as a basis for interpolation to a total of 32 images, which were again optimized using NEB. One of the three equivalent OH bonds pointing into the electronic cloud of the excess electron was chosen as that to be dissociated. These NEB calculations were performed using SIC-DFT. The resulting geometries plus independently optimized end points were used in a second NEB calculation with RI-MP2. DFT and RI-MP2 energies along the resulting MEPs are shown in the top panel of Fig. 7 together with snapshots of selected configurations. It is notable that the MEPs of the $H_3O(H_2O)_3$ dissociation with SIC-DFT and RI-MP2 are now much closer to each other in energy compared to those of the dissociation of the bare H_3O moiety. DFT performs well in the reaction region and for the barrier height, while slightly overstabilizing the products. The improved performance of DFT upon increasing the cluster size (and thus enhancing hydrogen bonding interactions) indicates applicability of this method for large clusters and the condensed phase. The bottom panel of Fig. 7 shows distances between atoms, defined the same way as before. The selected interatomic distances again change appreciably only in the vicinity of the transition state. Closer inspection of the geometries in the reactive region (for animation of the

reaction see Supplementary Material) reveals that the initial part of the reaction entails an overall compression of the cluster on the side of the hydrated electron. Only after this compression can the proton transfer from the hydronium cation to the neighboring water molecule start, being closely followed by the transfer of the next proton from the water molecule to the center of the electronic cloud, where it forms a hydrogen atom.

It is useful to quantify the changes in the shape of the spin density of the system during the reaction. For this purpose, we evaluate the gyration tensor of the spin density and quantities derived from it, namely its principal moments s_x, s_y, s_z, the radius of gyration r_g, and relative shape anisotropy κ^2.[7] These are plotted as functions of the reaction coordinate in Fig. 8. The spatial extent of the spin density, as measured by its radius of gyration, decreases monotonically during the reaction. The principal axes of the ellipsoid corresponding to the gyration tensor show a transition from an oblate shape in the initial state to a prolate shape during the reaction and finally to the spherical shape of a hydrogen atom in the final stage. The relative shape anisotropy, which is calculated from the principal moments, demonstrates that the asymmetry of the spin density reaches its maximum just after the transition state when the hydrogen atom is being formed. It is notable that the reactive process in a model system with only three water molecules already has all the properties of the reaction identified in a much larger cluster of 32 water molecules at a finite temperature.[7] The effect of the finite temperature in those cluster systems does not change the qualitative picture of the reaction mechanism in the $H_3O(H_2O)_3$ cluster. Note that this reaction has been observed and investigated, although not in such mechanistic detail, in small clusters theoretically[3,6] and it has been invoked in interpreting measurements of kinetic energy distributions of H-fragments for water nanoparticles doped with hydrogen halides.[4,6]

For additional insight into the concerted proton transfer, we have performed a two-dimensional relaxed PES scan in the space of the two OH bonds that are being broken. The surface is shown in Fig. 9 together with points corresponding to geometries from the NEB calculation. There is an apparent curved pathway, which is exemplified by the NEB curve, leading from the initial minimum to the transition state.

In Fig. 10, we compare calculations at the MEP geometries for the $H_3O(H_2O)_3$ cluster with different DFT settings in order to better understand the influence of the SIC and basis sets extensions. Energies for the DFT setup that was also used for the optimization of the NEB (SIC(a=0.3, b=0.2), molopt-TZV2P+ggg) are shown in blue. We have already established that these compare well to RI-MP2 energies (Fig. 7), therefore the reaction path thus obtained should be a good approximation to that optimized with RI-MP2. We further note that RI-MP2 energies match full MP2 energies to within less than 1 meV, which justifies the use of the RI approx-

imation for these calculations. Focusing first on the influence of basis set choice in our DFT calculations, we can see that the removal of diffuse basis functions (cyan) destabilizes reactants by about 0.6 eV and practically removes the barrier (0.02 eV). Comparison of the molopt-TZV2P+ggg basis set to an aug-TZV2P basis (not shown) indicates comparable overall quality of the augmentation with diffuse functions, with variations in relative energies in the 10 meV range. Setting the SIC parameters is also important. Using the original parameters a=0.2, b=0.0[26] (green) introduces an overall bias, overstabilizing products by roughly 0.45 eV when compared to SIC(a=0.3, b=0.2). Not using the SIC at all (red) reshapes the PES significantly, reducing the reaction exothermicity roughly to zero, and introduces an additional spurious and rather broad barrier. This is a severe change when compared to the roughly 0.7 eV decrease in energy between reactants and products with the optimized SIC(a=0.3, b=0.2). Finally, note the rather accidental compensation of errors between the self-interaction error and insufficient basis set in a calculation that uses only the molopt-TZV2P basis set and no SIC (gray).

4 Conclusions

We investigated by means of ab initio calculations how the radical character and reactivity of the H_3O species changes upon hydration by 1–3 water molecules. The first solvating water molecule has only a minor effect on the radical character of H_3O when accepting a hydrogen bond from it and virtually no effect when donating a hydrogen bond. As in the gas phase, in this smallest cluster with water H_3O remains a localized radical, which is metastable with respect to the loss of a hydrogen atom. The situation changes dramatically upon adding a second water molecule, which results in transfer of most of the spin density from H_3O to the solvent. Upon adding a third water molecule this transfer is practically completed and the cluster forms a solvent separated $H_3O^+ \cdots e^-$ pair. Microhydration thus completely alters the electronic character of the H_3O moiety from a localized radical to an H_3O^+ cation separated by water molecules from a hydrated electron. This change has consequences also for reactivity, which in the larger cluster proceeds as a proton transfer to the excess electron, forming a hydrogen atom. Both the electronic structure and the reaction path in the cluster with three water molecules already bear all the salient features of the situation in the aqueous bulk.

5 Acknowledgements

Support from the Czech Science Foundation (grants 203/08/0114), the Czech Ministry of Education (grant LC512), and the Academy of Sciences (Praemium Academie) is gratefully acknowledged. OM and FU acknowledge support from the IMPRS Dresden.

References

[1] A. L. Sobolewski and W. Domcke, *Journal of Physical Chemistry A*, 2002, **106**, 4158–4167.

[2] A. L. Sobolewski and W. Domcke, *Physical Chemistry Chemical Physics*, 2002, **4**, 4–10.

[3] A. L. Sobolewski and W. Domcke, *Physical Chemistry Chemical Physics*, 2007, **9**, 3818–29.

[4] V. Poterya, M. Farnik, P. Slavicek, U. Buck and V. V. Kresin, *Journal of Chemical Physics*, 071101–071104.

[5] V. Poterya, M. Farnik, M. Oncak and P. Slavicek, *Physical Chemistry Chemical Physics*, 2008, **10**, 4835–4842.

[6] V. Poterya, J. Fedor, A. Pysanenko, O. Tkac, J. Lengyel, M. Oncak, P. Slavicek and M. Farnik, *Phys. Chem. Chem. Phys.*, 2011, **13**, 2250–2258.

[7] O. Marsalek, T. Frigato, J. VandeVondele, S. E. Bradforth, B. Schmidt, C. Schütte and P. Jungwirth, *The Journal of Physical Chemistry B*, 2009, **114**, 915–920.

[8] B. C. Garrett, D. A. Dixon, D. M. Camaioni, D. M. Chipman, M. A. Johnson, C. D. Jonah, G. A. Kimmel, J. H. Miller, T. N. Rescigno, P. J. Rossky, S. S. Xantheas, S. D. Colson, A. H. Laufer, D. Ray, P. F. Barbara, D. M. Bartels, K. H. Becker, H. Bowen, S. E. Bradforth, I. Carmichael, J. V. Coe, L. R. Corrales, J. P. Cowin, M. Dupuis, K. B. Eisenthal, J. A. Franz, M. S. Gutowski, K. D. Jordan, B. D. Kay, J. A. LaVerne, S. V. Lymar, T. E. Madey, C. W. McCurdy, D. Meisel, S. Mukamel, A. R. Nilsson, T. M. Orlando, N. G. Petrik, S. M. Pimblott, J. R. Rustad, G. K. Schenter, S. J. Singer, A. Tokmakoff, L. S. Wang, C. Wittig and T. S. Zwier, *Chemical Reviews*, 2005, **105**, 355–389.

[9] D. M. Bartels, M. T. Craw, P. Han and A. D. Trifunac, *Journal of Physical Chemistry*, 1989, **93**, 2412–2421.

[10] D. M. Bartels, A. R. Cook, M. Mudaliar and C. D. Jonah, *Journal of Physical Chemistry A*, 2000, **104**, 1686–1691.

[11] A. N. Alexandrova, *Journal of Physical Chemistry A*, 2010, **114**, 12591–12599.

[12] A. Wilson, T. vanMourik and T. Dunning, *Journal of Molecular Structure-Theochem*, 1996, **388**, 339–349.

[13] *TURBOMOLE V6.2 2010, a development of University of Karlsruhe and Forschungszentrum Karlsruhe GmbH, 1989-2007, TURBOMOLE GmbH, since 2007; available from* `http://www.turbomole.com`.

[14] R. Elber and M. Karplus, *Chemical Physics Letters*, 1987, **139**, 375–380.

[15] C. G. Broyden, *IMA Journal of Applied Mathematics*, 1970, **6**, 76–90.

[16] R. Fletcher, *The Computer Journal*, 1970, **13**, 317–322.

[17] D. Goldfarb, *Mathematics of Computation*, **24**, 23–26.

[18] D. Shanno, *Mathematics of Computation*, 1970, **24**, 647.

[19] E. Bitzek, P. Koskinen, F. Gähler, M. Moseler and P. Gumbsch, *Phys. Rev. Lett.*, 2006, **97**, 170201.

[20] G. Henkelman, B. Uberuaga and H. Jonsson, *Journal of Chemical Physics*, 2000, **113**, 9901–9904.

[21] S. R. Bahn and K. W. Jacobsen, *Comput. Sci. Eng.*, 2002, **4**, 56–66.

[22] M. Valiev, E. Bylaska, N. Govind, K. Kowalski, T. Straatsma, H. V. Dam, D. Wang, J. Nieplocha, E. Apra, T. Windus and W. de Jong, *Computer Physics Communications*, 2010, **181**, 1477 – 1489.

[23] A. Becke, *Physical Review A*, 1988, **38**, 3098–3100.

[24] C. Lee, W. Yang and R. Parr, *Physical Review B*, 1988, **37**, 785–789.

[25] S. Grimme, *Journal of Computational Chemistry*, 2006, **27**, 1787–1799.

[26] J. VandeVondele and M. Sprik, *Physical Chemistry Chemical Physics*, 2005, **7**, 1363–1367.

[27] VandeVondele, Joost and Hutter, Juerg, *Journal of Chemical Physics*, 2007, **127**, 114105.

[28] O. Marsalek, F. Uhlig and P. Jungwirth, *Structure, dynamics, and reactivity of hydrated electrons by ab initio*

molecular dynamics, submitted.

[29] S. Goedecker, M. Teter and J. Hutter, *Physical Review B*, 1996, **54**, 1703–1710.

[30] L. Genovese, T. Deutsch, A. Neelov, S. Goedecker and G. Beylkin, *Journal of Chemical Physics*, 2006, **125**, 074105.

[31] G. Henkelman and H. Jonsson, *Journal of Chemical Physics*, 2000, **113**, 9978–9985.

[32] K. W. J. H. Jonsson, G. Mills, *Classical and Quantum Dynamics in Condensed Phase Simulations*, World Scientific, 1998.

[33] J. VandeVondele, M. Krack, F. Mohamed, M. Parrinello, T. Chassaing and J. Hutter, *Computer Physics Communications*, 2005, **167**, 103–128.

[34] S. K. Chulkov, N. F. Stepanov and Y. V. Novakovskaya, *Russian Journal Physical Chemistry A*, 2009, **83**, 798–808.

	VIP [eV]
(A) H_3O	5.88
(B) $H_3O(H_2O)_1$	5.65
(C) $H_3O(H_2O)_1$	4.56
(D) $H_3O(H_2O)_2$	4.11
(E) $H_3O(H_2O)_3$	4.09

Table 1: Vertical ionization potentials for the five structures depicted in Fig. 1.

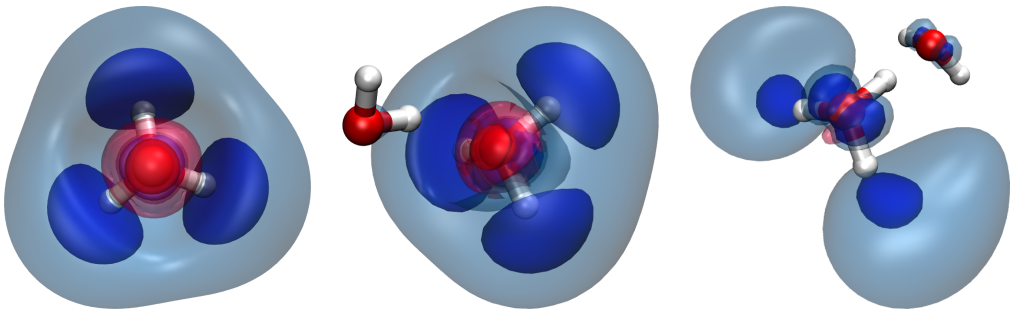

(A) H_3O (B) $H_3O(H_2O)$ (C) $H_3O(H_2O)$ eV

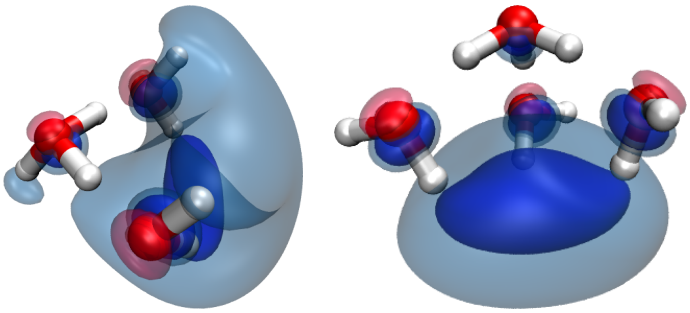

(D) $H_3O(H_2O)_2$ (E) $H_3O(H_2O)_3$

Figure 1: Minimum energy structures of the $H_3O(H_2O)_n$ (n= 0 ... 3) clusters. Depicted are contours of the spin density at four different values ($\pm$ 0.001 and $\pm$ 0.003 e $\cdot$ Bohr^{-3})

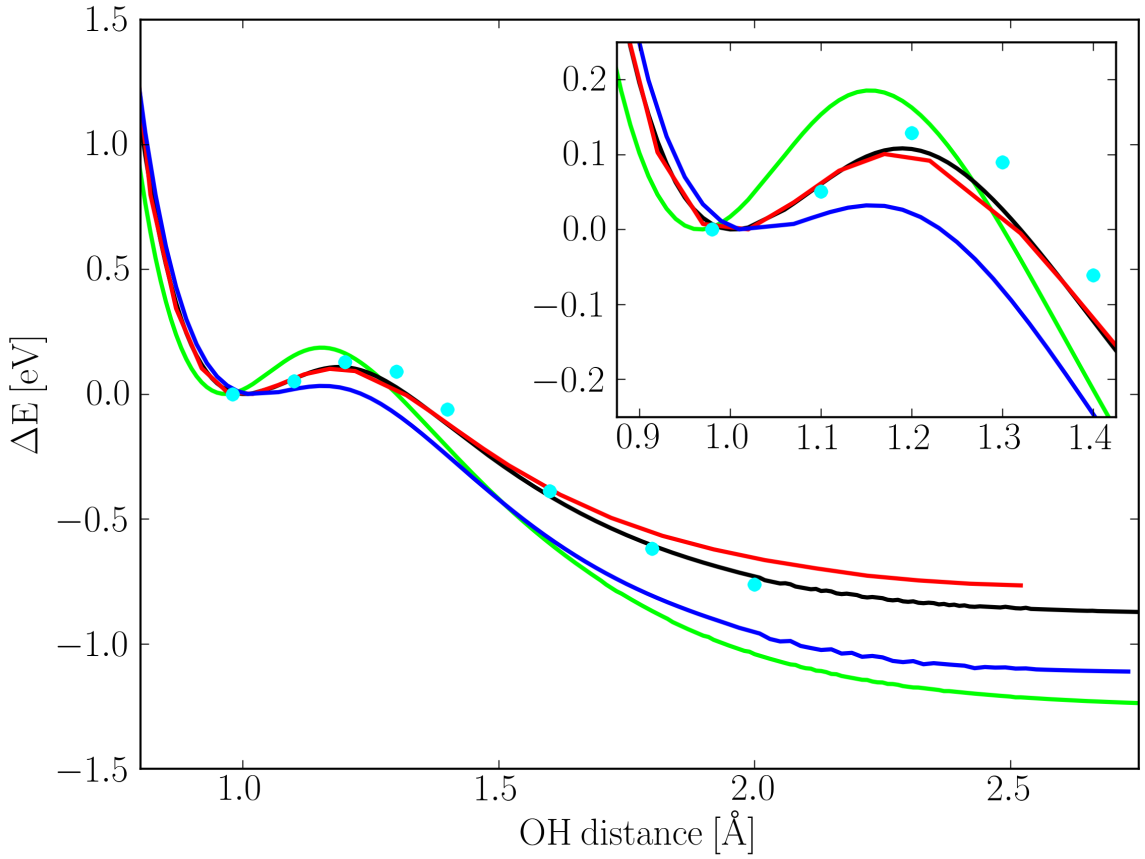

Figure 2: Minimum energy paths for OH bond dissociation in a hydronium radical. Relaxed scan obtained with RI-MP2 (black) with the aug-cc-pVTZ basis set. Energies of the RI-MP2 geometries calculated with UHF with the aug-cc-pVTZ basis set (green), CCSD(T) with the aug-cc-pVTZ basis set (red) and SIC-DFT (a=0.3, b=0.2) with the molopt-TZV2P+ggg basis (blue). CASPT2 (cyan dots) energies calculated with the double-ζ ANO-L split valence basis set augmented with additional diffuse s and p functions on the oxygen atoms ($\zeta = 0.02\,\mathrm{Bohr}^{-1}$) are shown. The CASPT2 energies are taken from ref. 2

.

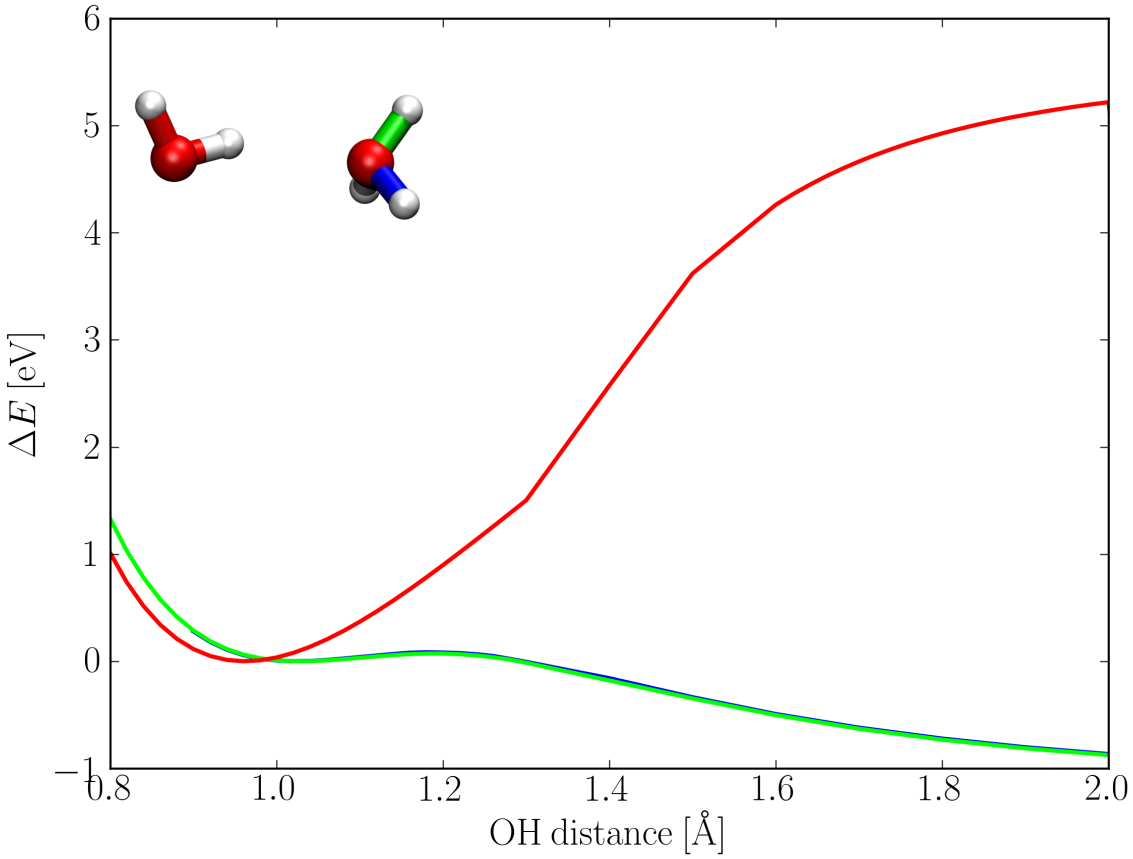

Figure 3: Minimum energy paths for different OH bond dissociations in the $H_3O(H_2O)$ (B) cluster. Inset shows the minimum structure of the cluster. The color coding of the curves corresponds to colors of the bonds of the structure displayed.

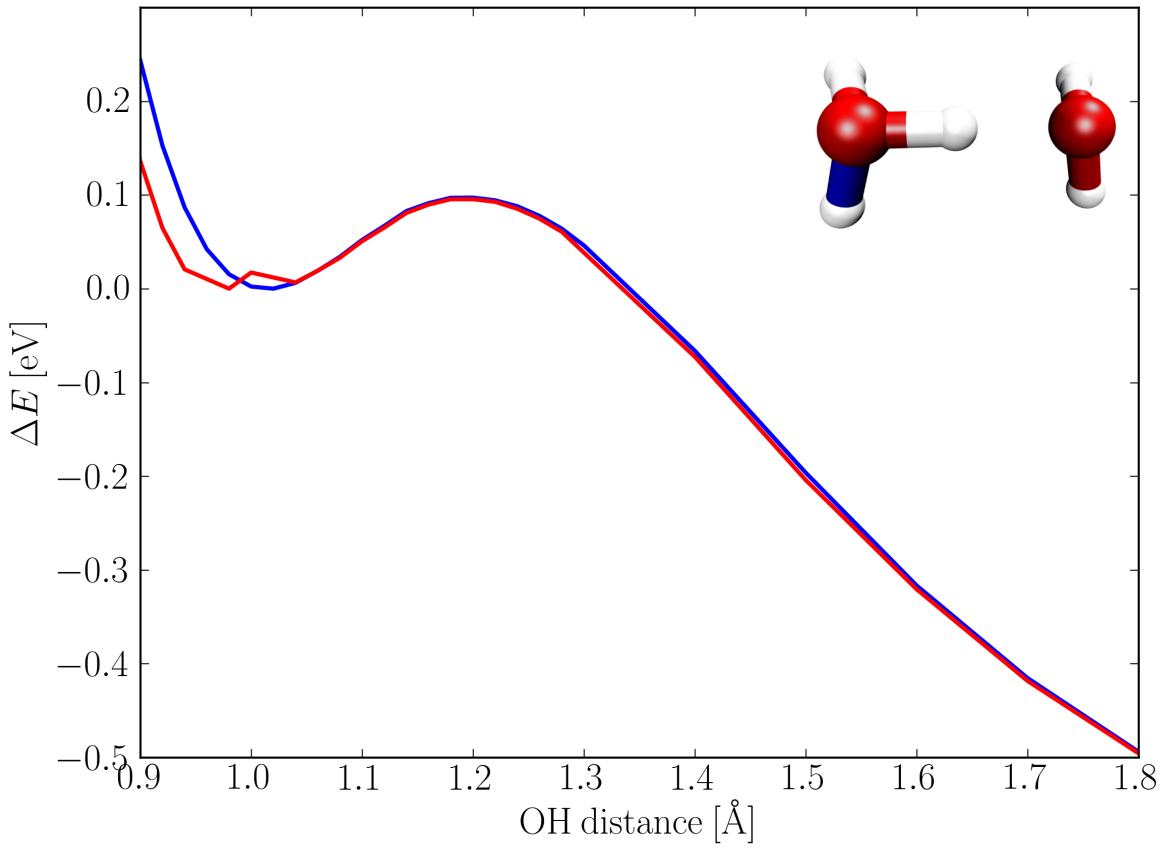

Figure 4: Minimum energy paths for different OH bond dissociations in the $H_3O(H_2O)$ (C) cluster. Inset shows the minimum structure of the cluster. The color coding of the curves corresponds to colors of the bonds of the structure displayed.

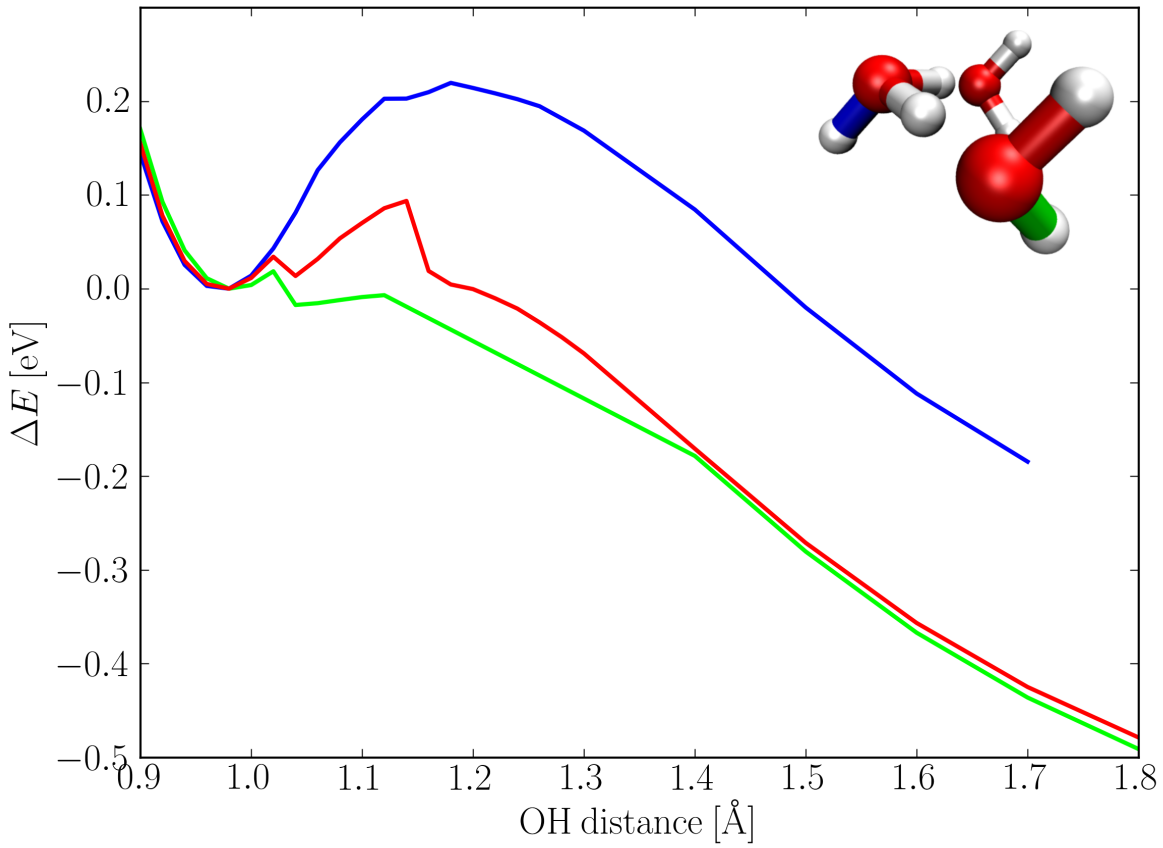

Figure 5: Minimum energy paths for different OH bond dissociations in the $H_3O(H_2O)_2$ (D) cluster. Inset shows the minimum structure of the cluster. The color coding of the curves corresponds to colors of the bonds of the structure displayed.

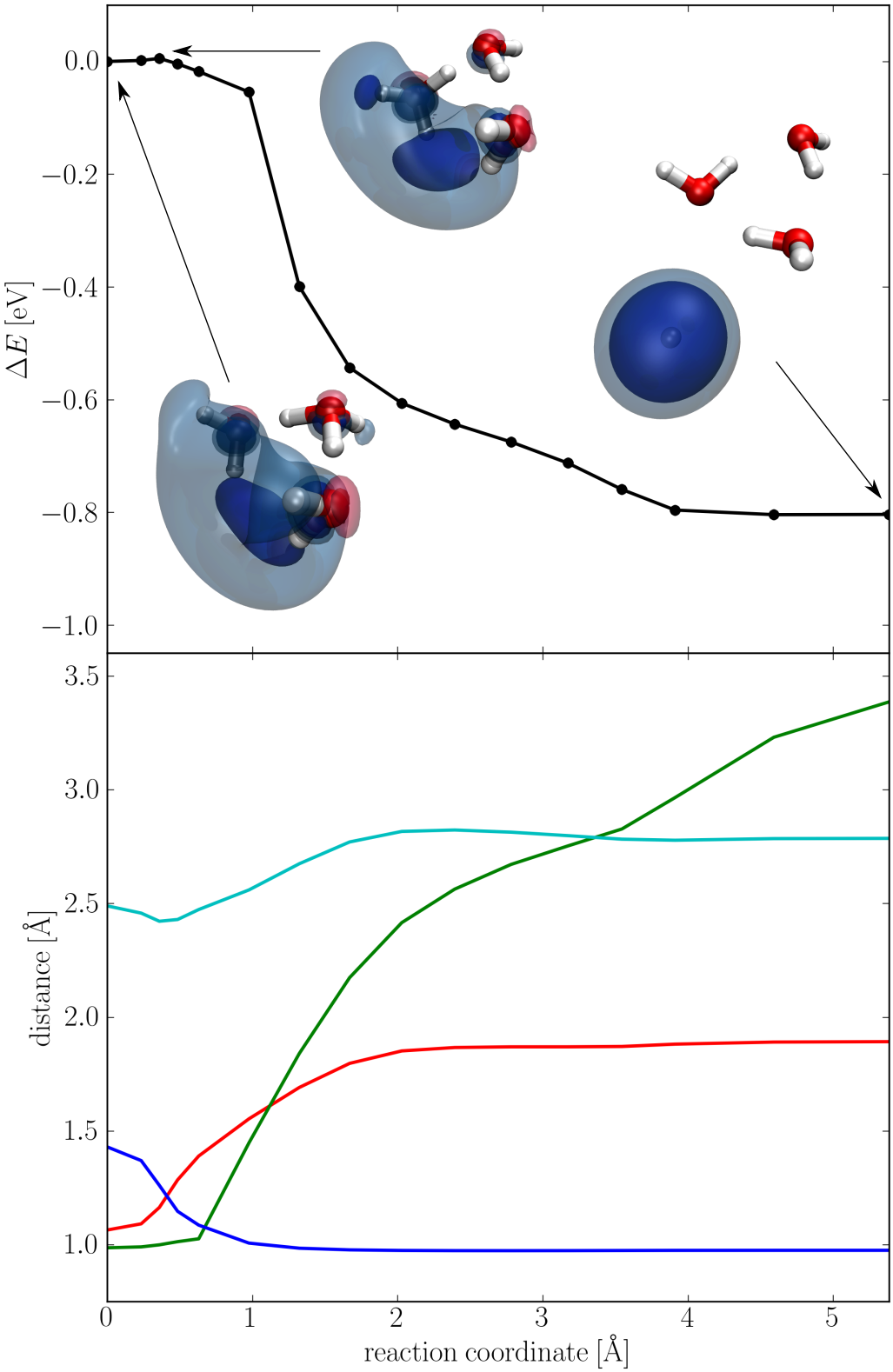

Figure 6: MEP for $H_3O(H_2O)_2$ obtained with NEB and RI-MP2 and aug-cc-pVTZ basis set (top panel). Bottom panel shows distances of OH in hydronium cation (red), OH distance in water molecule (green), OO distance of before mentioned molecules (cyan) and OH distance in newly formed water molecule (blue).

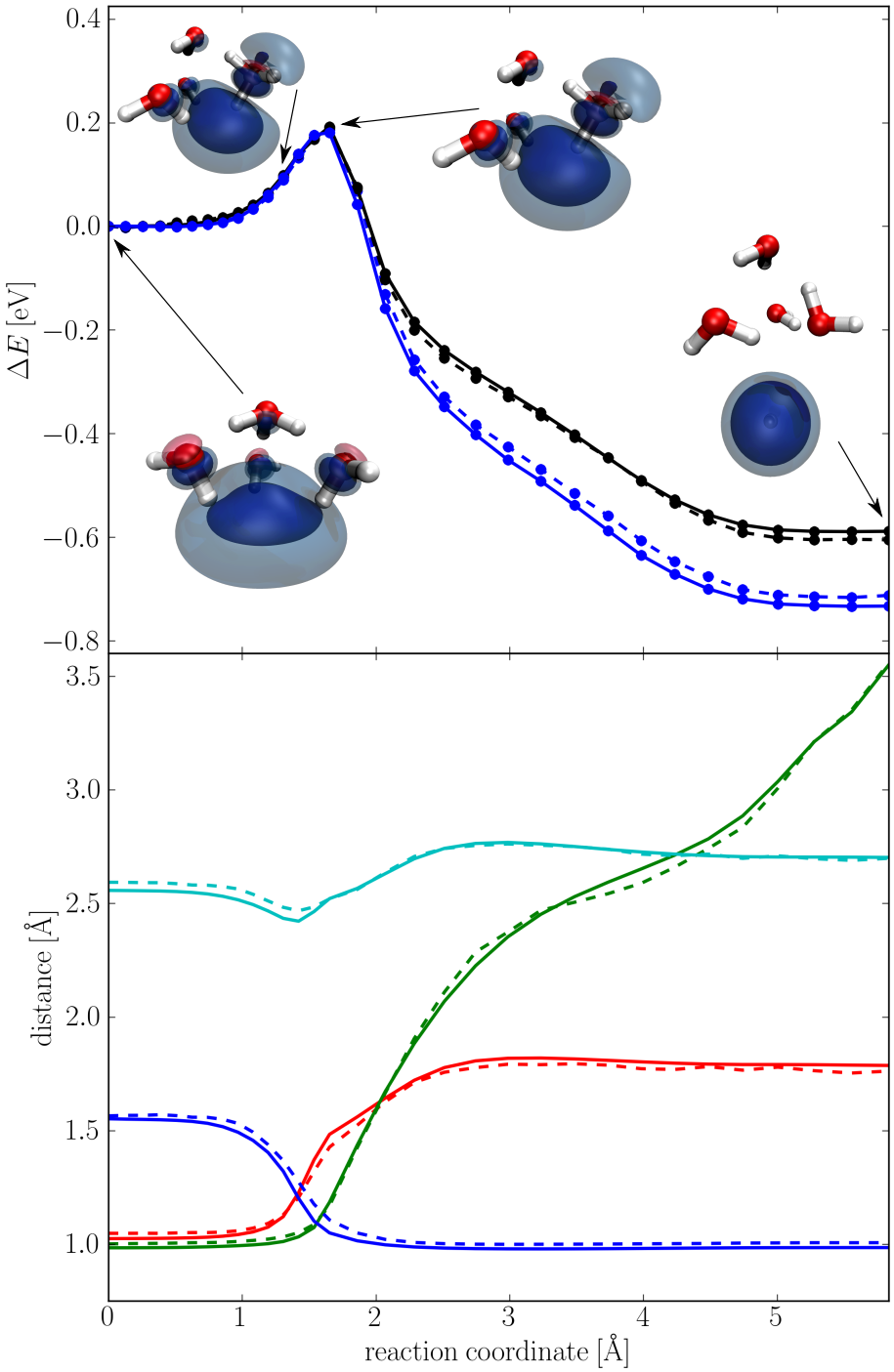

Figure 7: Two MEPs for $H_3O(H_2O)_3$ obtained with NEB optimized using two different electronic structure setups. SIC-DFT (a=0.3, b=0.2) using the molopt-TZV2P+ggg basis set is shown in blue in top panel, RI-MP2 using the aug-cc-pVTZ basis set is shown in black. Energies at DFT and RI-MP2 geometries are shown using dashed and full lines, respectively. Bottom panel shows distances of OH in hydronium cation (red), OH distance in water molecule (green), OO distance of before mentioned molecules (cyan) and OH distance in newly formed water molecule (blue) from the DFT and RI-MP2 calculations using dashed and full lines, respectively.

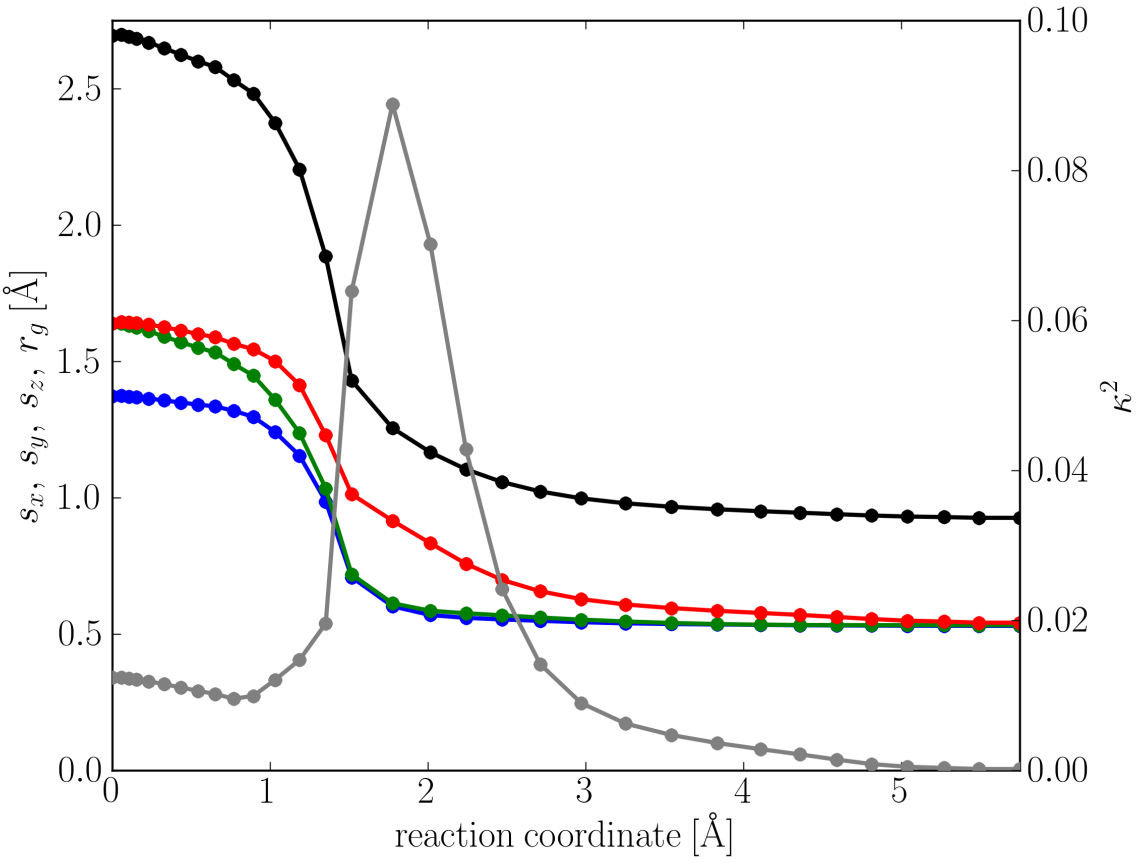

Figure 8: Principal moments s_x, s_y and s_z of gyration tensor of the spin density along the MEP obtained with NEB calculations (red, green, blue). Radius of gyration r_g in black and relative shape anisotropy κ^2 in gray.

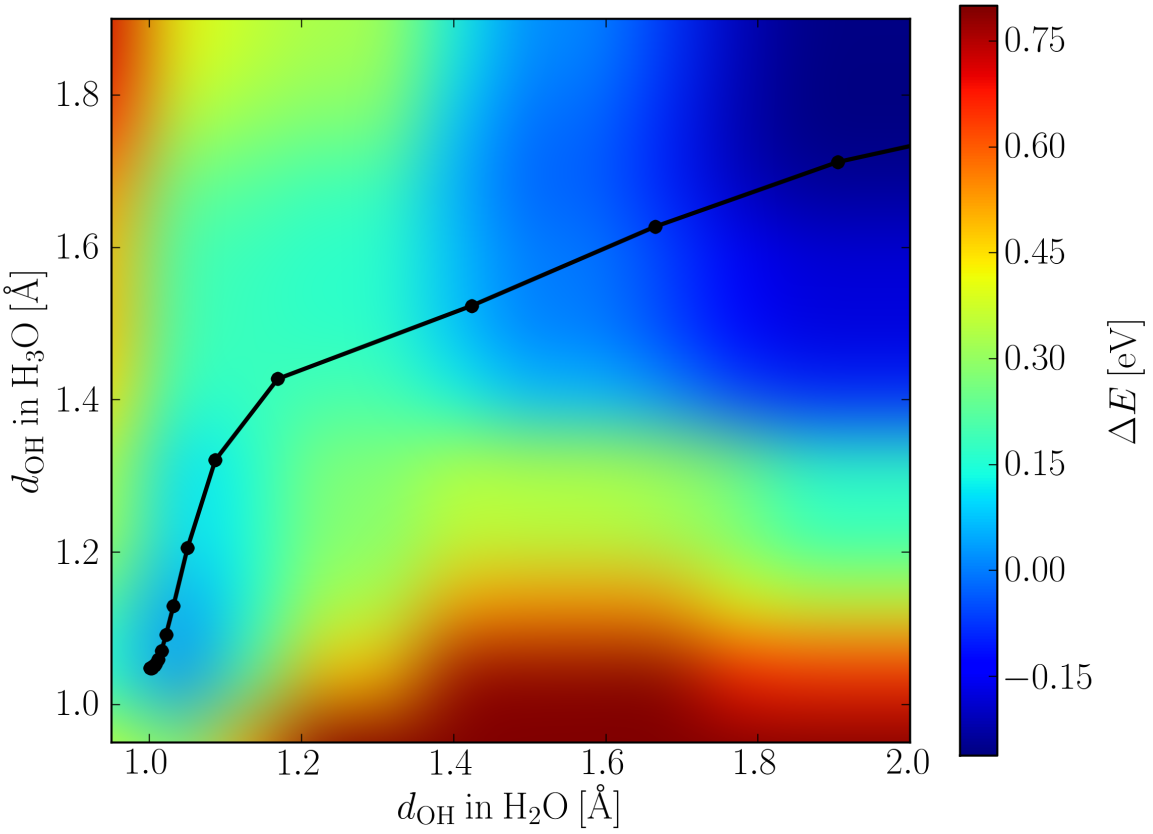

Figure 9: Two-dimensional relaxed PES scan for $H_3O(H_2O)_3$ along OH bond distance in H_3O cation and OH bond distance in water molecule hydrogen-bonded to H_3O at corresponding OH bond (colored). Black dots are at values of the OH bond lengths at the geometries of the MEP obtained with NEB calculations.

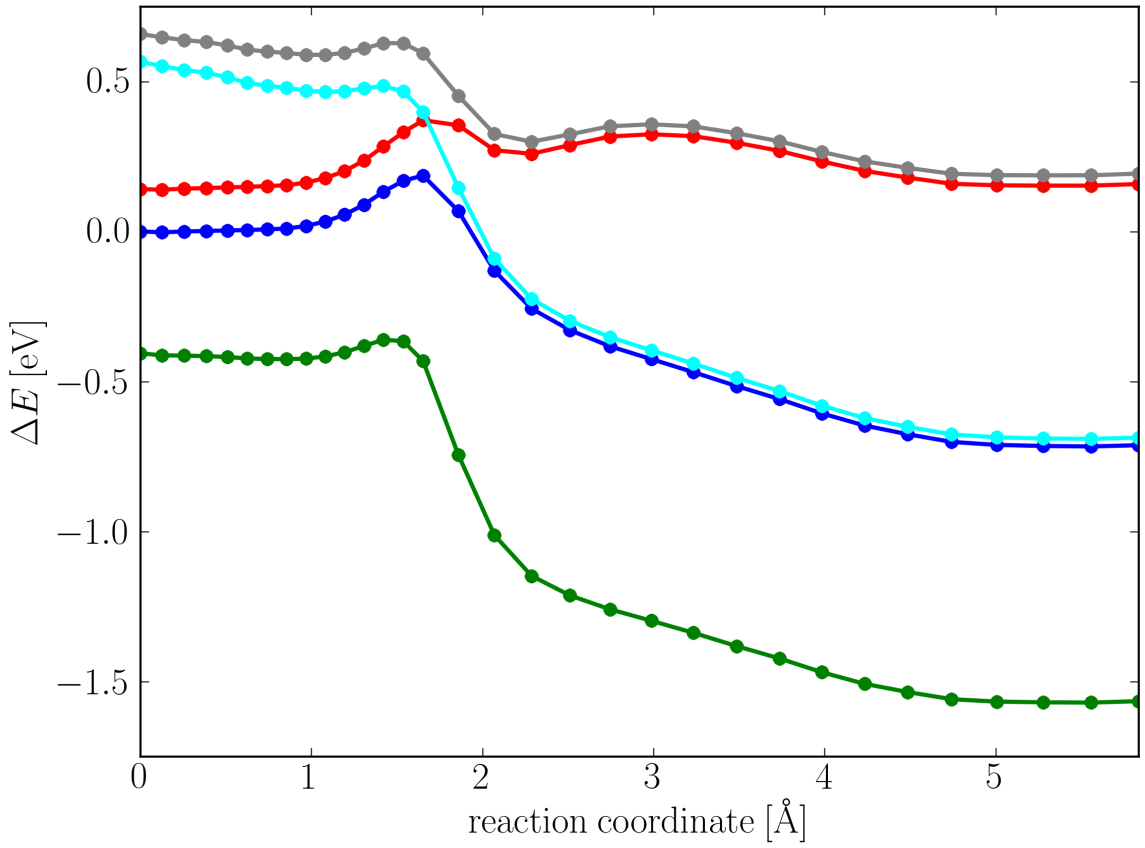

Figure 10: Energies of the $H_3O(H_2O)_3$ cluster obtained using DFT with different basis sets and settings of the SIC calculated along the same MEP as shown in Fig 7 (obtained with molopt-TZV2P+ggg basis set and SIC(a=0.3, b=0.2), blue). Energies with molopt-TZV2P+ggg and SIC(a=0.2, b=0.0) are shown in green, with molopt-TZV2P+ggg and no SIC in red, with molopt-TZV2P and SIC(a=0.3, b=0.2) in cyan and with molopt-TZV2P and no SIC in gray.